High On−Off Conductance Switching Ratio in Optically-Driven Self-Assembled Conjugated Molecular Systems

ARTICLE *in* ACS NANO · MARCH 2010

Impact Factor: 12.88 · DOI: 10.1021/nn100295x · Source: PubMed

10 AUTHORS, INCLUDING:

Smaali Kacem
Université des Sciences et Technologies de…
36 PUBLICATIONS **220** CITATIONS
SEE PROFILE

Sylvie Godey
Autonomous University of Barcelona
52 PUBLICATIONS **394** CITATIONS
SEE PROFILE

Alain Rochefort
Polytechnique Montréal
88 PUBLICATIONS **1,941** CITATIONS
SEE PROFILE

Jean Roncali
French National Centre for Scientific Resea…
349 PUBLICATIONS **14,610** CITATIONS
SEE PROFILE

High On−Off Conductance Switching Ratio in Optically-Driven Self-Assembled Conjugated Molecular Systems

Kacem Smaali,[†] Stéphane Lenfant,[†,*] Sandrine Karpe,[‡] Maïténa Oçafrain,[‡] Philippe Blanchard,[‡] Dominique Deresmes,[†] Sylvie Godey,[†] Alain Rochefort,[§] Jean Roncali,[‡] and Dominique Vuillaume[†,*]

[†]Molecular Nanostructures & Devices Group, Institute for Electronics Microelectronics and Nanotechnology, CNRS & University of Lille, B.P. 60069, 59652, Villeneuve d'Ascq, France, [‡]Linear Conjugated Systems Group, CNRS, CIMA, University of Angers, 2 Bd Lavoisier, 49045, Angers, France, and [§]Département de génie physique, École Polytechnique de Montréal, Montréal, Canada H3C 3A

ABSTRACT A new azobenzene−thiophene molecular switch is designed, synthesized, and used to form self-assembled monolayers (SAM) on gold. An "on/off" conductance ratio up to 7×10^3 (with an average value of 1.5×10^3) is reported. The "on" conductance state is clearly identified to the cis isomer of the azobenzene moiety. The high on/off ratio is explained in terms of photoinduced, configuration-related changes in the electrode−molecule interface energetics (changes in the energy position of the molecular orbitals with respect to the Fermi energy of electrodes) in addition to changes in the tunnel barrier length (length of the molecules). First principles density functional calculations demonstrate a better delocalization of the frontier orbitals as well as a stronger electronic coupling between the azobenzene moiety and the electrode for the cis configuration over the trans one. Measured photoionization cross sections for the molecules in the SAM are close to the known values for azobenzene derivatives in solution.

KEYWORDS: molecular switch · azobenzene · self-assembled monolayer · molecular electronics · charge transport · first principles

The immobilization of π-conjugated systems with electro-optical properties on gold surfaces by formation of self-assembled monolayers (SAMs) is the focus of high interest.[1] Reversible photoswitching devices were demonstrated with diarylethene and azobenzene derivatives[2] and open the route for potential applications as optical switches in molecular electronics,[3−7] molecular machines,[8] photoswitchable surface wettability,[9,10] and biosensors.[11] Azobenzene molecules were extensively studied for their unique photoisomerization behavior. These molecules show a transition from a more thermodynamically stable trans configuration to a cis configuration upon exposure to UV light (~360 nm), and a reversible isomerization under blue light (~480 nm). The properties of azobenzenes in solution (*e.g.*, robust reversible photoisomerization, long living states, fast switching) make them promising building blocks for molecular-scale devices and nanotechnology.

It is well-known that photoisomerisable molecules need to be electronically decoupled from the metal surface to properly work, that is, to reversibly switch between the two isomers. Scanning tunnel microscopy (STM) experiments on a single azobenzene molecule physisorbed on gold show that reversible switching is only observed when *tert*-butyl legs lift the molecule up.[12] In several works using SAMs, the photoisomerizable molecules are chemically attached to the substrate using various spacers: short alkyl chains (2−6 carbon atoms),[3,13,14] ethylene bond,[7] or phenyl or thiophene moieties.[2,4,8,15,16] The role of this linker is crucial. In the case of diarylethene, the observation of reversible switching depends on its nature (*e.g.*, phenyl *vs* thiophene).[16] Contradictory, some authors associate the higher "on" conductance state to the trans isomer,[3,7,14,17−20] while others conclude in favor of the cis form.[4,8,12] In some cases, this discrepancy can be accounted for by a different geometrical orientation of the molecules (lying flat on the substrate[12] or almost normal oriented), but the contradiction still holds for the same orientation (*e.g.*, approximately standing upright normal to the electrode surface; see for instance refs 17, 21). Moreover, up to now, azobenzene derivatives have not exhibited a clear intrinsic conductance switching. The apparent change in the measured conductance has been attributed to a change in the length of the molecule during the isomerization rather than to an intrinsic conductance switching associated with changes in the electronic structure of the molecular junction.[4,8] Many reasons can explain these results; details on the molecular arrangements in the monolayers and

*Address correspondence to dominique.vuillaume@iemn.univ-lille1.fr, stephane.lenfant@iemn.univ-lille1.fr.

Received for review February 12, 2010 and accepted March 19, 2010.

Published online March 29, 2010.
10.1021/nn100295x

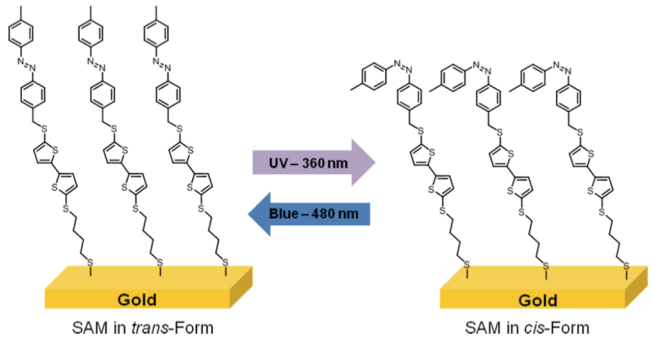

Figure 1. Schematic view of the SAM with the AzBT molecules in the trans and cis isomers.

the nature of the coupling between the molecule and the electrode contact are among the most important factors that can influence the electrical behavior. For instance, Cuniberti *et al.*[17,21] showed by first principles calculations that $G_{trans} > G_{cis}$ when the azobenzene is chemically linked between two carbon nanotube electrodes, while $G_{cis} > G_{trans}$ in case of silicon electrodes (G_{trans} and G_{cis} are the conductances of the junction for the trans and cis isomers, respectively). Obviously, the role of the spacer is also critical. A short spacer should favor the electron transfer rate through the junction and increase its conductance, while a longer spacer could improve the decoupling of the azobenzene moiety from the substrate, thus allowing a larger dynamic of the switching event, and thus a larger on/off conductance ratio.

Here, we report the electrical properties of a new molecular switch in which the azobenzene moiety is linked to a bithiophene spacer and a short (4 carbon atoms) alkanethiol. Such a design is expected to combine the benefit of a rather long spacer, while preserving a sufficiently high level of current due to the presence of the electron-rich bithiophene unit (compared to a fully saturated spacer with the same length). The effects of the reversible photoisomerization on the SAM thickness, surface wettability, and electrical conductivity are analyzed. The photoinduced changes in the conductance of the SAM are mainly investigated by conducting AFM (C-AFM). A record on/off ratio up to 7×10^3 between the cis (on) and trans (off) configurations is demonstrated. The analysis of these results using well-established electron transport models and molecular frontier orbitals from first principles density function theory (DFT) calculations indicates that this high photoinduced on/off ratio results from a synergistic combination of SAM thickness variation and modification of the energy offset between the lowest unoccupied molecular orbital (LUMO) and the electrode Fermi energy. We also report photoionization cross sections for these molecules embedded in the molecular junctions on a par with known values for azobenzene and derivatives in solution.

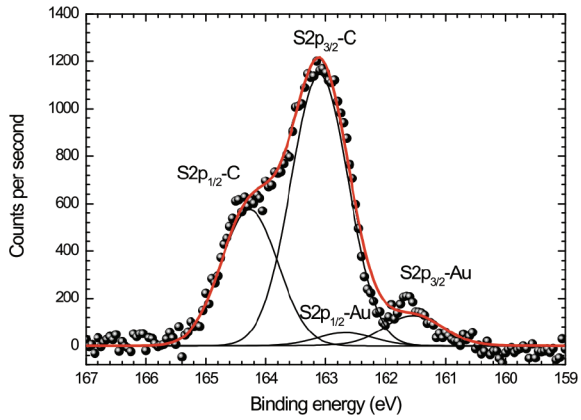

Figure 2. Curve-fitted high-resolution XPS spectra for the S_{2p} region of SAM grafted on a gold surface. The apparition of two doublets is due to the presence of sulfur atoms linked with gold atoms or linked with carbon atoms, and each doublet results from the spin−orbit splitting of the S_{2p} level.

DISCUSSION AND RESULTS

Monolayer Formation and Characterization. The new azobenzene-bithiophene derivative (AzBT) was synthesized and used to form self-assembled monolayers (SAM) by chemisorption on gold surfaces (Figure 1) (see Experimental Section). The SAMs were structurally characterized and all these measurements converge to identify the presence of dense monolayers of the desired molecules (4×10^{-10} mol/cm^2 or 2.4×10^{14} molecules/cm^2 or 1 molecule *per* 41 Å^2 as determined by cyclic-voltammetry (CyV) measurements, see Experimental Section). The entire X-ray photoemission spectroscopy (XPS) spectrum (not shown here) of the functionalized surface shows the presence of the different atoms of the molecule: carbon (peak C_{1s}), nitrogen (peak N_{1s}), and sulfur (peaks S_{2s} and S_{2p}). The C_{1s} spectrum shows one component attributed to C−C at 284.3 eV. This peak position is in good agreement with results published for monolayers grafted on gold where the position of the C−C peak has been measured at 284.6 eV.[22−24] The other peak positions (N_{1s} and S_{2s}) appear at 399.5 eV and 227.4 eV, respectively. The ratio of the corrected peak area N_{1s}/C_{1s} was about 0.082, a value close to the expected value 2/26 = 0.077 (2 nitrogen atoms and 26 carbon atoms per molecule). The high resolution XPS spectra for the S_{2p} region shows two doublets (Figure 2). Each doublet results from the spin−orbit splitting of the S_{2p} level and consists of a high-intensity $S_{2p3/2}$ peak at lower energy and a low-intensity $S_{2p1/2}$ peak at higher energy separated by 1.2 eV with an intensity ratio of 2/1.[22] The value of the $S_{2p3/2}$ peak at 161.5 eV for the SAM is in agreement with the binding energy for bound alkanethiolate on gold (161.9−162.0 eV).[25,26] Thus, peaks at 161.5 and 162.7 eV of the lower-energy doublet $S_{2p3/2,1/2}$ of SAM may be assigned to the thiol chemisorbed on the Au surface.[22,27] The other doublet, $S_{2p3/2,1/2}$, at respectively 163.1 and 164.3 eV corresponds to other sulfur atoms in the body of the molecule (thiophene). The comparison of the areas of these two doublet signals leads to an es-

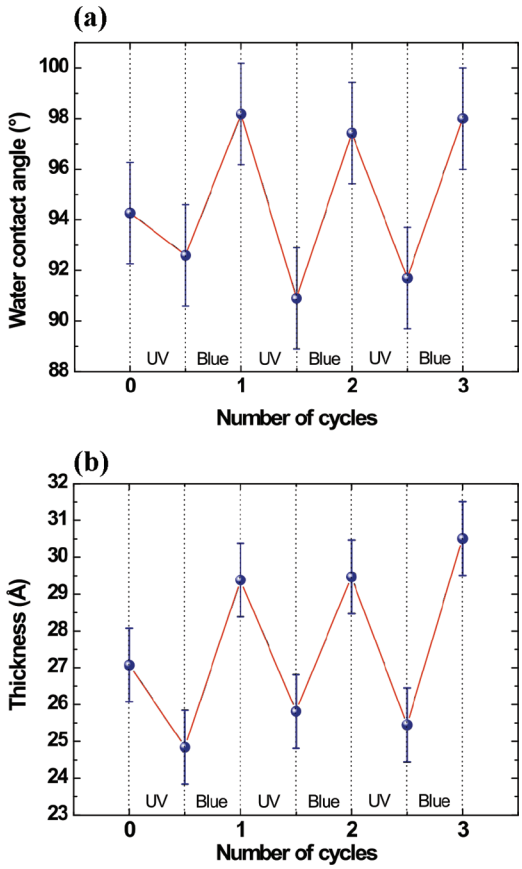

Figure 3. (a) Evolution of the water contact angle of the SAM and (b) evolution of the thickness of the SAM measured by spectroscopic ellipsometry as a function of the irradiation during three cycles. After formation, the SAM was alternatively exposed to UV light (360 nm) and visible light (480 nm) during 90 min.

timated S−C/S−Au ratio of 6.2 ± 2.0 which is compatible with the expected value (S−C/S−Au = 4) for one sulfur atom linked to the gold surface *versus* four sulfur atoms linked with carbon atoms in the molecule.

We focalized UV-light (360 nm) and blue light (480 nm) on the SAM from a xenon lamp through an optical fiber (see Experimental Section). We followed the evolution of the water contact angle of the SAM as a function of the light irradiation wavelength (Figure 3). Before light irradiation, the contact angle on the SAM is 94 ± 2°. After UV irradiation (trans-to-cis isomerization) during 90 min, the contact angle decreases to ~92 ± 2°, and switches back to a higher value (~98 ± 2°) after blue irradiation (cis-to-trans isomerization). This behavior is reproducible. The intermediate value for the pristine SAM can be explained by the fact that the SAM after its formation is composed of a mix of cis and trans isomers. The difference of wettability between the two isomers is due to several reasons: (i) In the trans form, the surface of the SAM is mainly composed of CH_3 groups, while with the molecules in the cis form, the surface exposes mainly the N═N bonds and the phenyl groups. (ii) Difference in the molecule dipole: the dipole moment of the cis isomer is higher than the trans isomer (for our molecule μ_{cis} = 4.9D and μ_{trans} = 1.8D from MOPAC calculations).[28] This variation of the contact angle between the two isomers, $\Delta\theta = 6 \pm 2°$, is close to those measured on other azobenzene systems.[9,29]

Similarly, Figure 3b shows the variations of the thickness for the SAM with molecules in the cis and trans isomers. The average thickness of the SAM after blue light exposure (trans isomer) is d_{trans} = 30 ± 1 Å and d_{cis} = 25 ± 1 Å after UV-light exposure (cis isomer). We compared these thicknesses with the lengths of the molecule calculated by MOPAC.[28] The length for the molecule in cis and trans forms is estimated at ~26 and 31 Å, respectively. These values are very close to measured ones. The thickness of the pristine SAM is intermediate between the thickness of the SAM with molecules in their cis and trans conformations. This feature is consistent with a SAM composed of a mix of cis and trans isomers, as observed for the contact angle measurement above. The difference of thickness (here ~5 Å) is consistent with other results on azobenzene monolayers.[4,6,8,9,30] We can crudely estimate the ratio of cis/trans isomers in the pristine SAM by considering that the measured thickness is proportional to the relative amount of both isomers ($d = \eta d_{cis} + (1 - \eta) d_{trans}$) as previously done in binary SAMs of alkylchains with two different lengths.[31] We get ~55% of cis isomers (with a relative accuracy of 25% corresponding to the ±1 Å error bar of the ellipsometer measurements). Similarly, the fact that the measured thicknesses after a long exposure to UV-light (blue, respectively) (25 ± 1 Å, 30 ± 1 Å) are almost equal to the calculated length of the molecule in the cis (trans, respectively) configuration (~26 Å, ~31 Å) allow us to estimate that more than 75% of the molecules are in cis (trans, respectively) isomer after UV (blue, respectively) light exposures. Efficiency of the isomerization in the range 80−99% has been reported.[32] This switching behavior is reproducible and stable. We did not measured more than 10 switching events (due to time limitation, for instance the samples were exposed during 9 h in total during the three cycles of reversible isomerization shown in Figure 3). However, we do not observe any degradation of the SAM thickness during this exposure to light. This feature is confirmed by CyV showing no change in the surface coverage (2.4×10^{14} molecules/cm^2, see aforementioned) upon long time exposure to light. This result means that trans−cis isomerization occurs without rearrangement at the S−Au anchoring sites as already pointed out by more accurate STM experiments.[33] As in the case of molecules in solution, photoirradiation with 360 nm for 3 h did not lead to significant alteration of the CyV response suggesting (i) good stability of the monolayer under irradiation and (ii) that trans and cis isomers show similar electrochemical properties. We have also observed that these SAMs exhibit a long-term stability. The switching behavior

was still observed after a period of several months at rest in the dark and in a controlled atmosphere (dry nitrogen). Note also that the cis isomer is stable for a long period (more than 11 h) of rest in the dark with no recovering of the trans isomer (see Supporting Information). Finally, it is known that photoisomerization efficiency depends on the packing density in the SAM. No switching has been observed for densely packed SAMs of azobenzene derivatives functionalized with alkythiol chains,[34] while diluted SAMs of azobenzene derivatives in alkylthiol matrix have displayed photoisomerization behaviors.[20,34] On the other hand, other reports on close-packed SAMs based on single azobenzene derivatives have shown to present trans−cis isomerization,[4,8] and even a collective isomerization of entire molecular-crystalline domains.[33] In that later case, azobenzene derivatives are arranged in a densely packed (~29 Å^2 *per* molecule)[33] and crystalline architecture. However their herringbone 2D packing, governed mostly by π−π interactions, enabled the trans−cis isomerization. In our case, (i) the molecules are less packed (41 Å^2 *per* molecule, see above) allowing an easier isomerization; (ii) the presence of a conjugated bithiophene unit in molecule **1** (AzBT) may also generate π−π interactions that may contribute to collective switching as in ref 33, however STM imaging at molecular resolution will be further required to confirm this hypothesis.

Electrical Behavior at the Nanoscale. Current−voltage (*I*−*V*) curves were recorded by forming a junction with the metallic tip of a conducting-AFM (see Experimental Section). Typical *I*−*V* curves are presented in Figure 4 for a pristine SAM, after irradiation at 360 nm (for 90 min) to switch the molecules to the cis isomer, and after exposure to 480 nm light (for 90 min) to switch to the trans isomer. From these two later curves, a typical on/off ratio of ~10^3 is determined for this typical case ($|V| > 0.5$ V) irrespective of the bias polarity. For each configuration, we recorded a total of around 40 *I*−*V* traces (see Experimental Section). Histograms of the currents at −1.5 and 1.5 V are plotted (log-scale) in Figures 4b and 4c, respectively. The current distribution follows a log-normal distribution as also observed for alkanethiol SAMs.[35] In the framework of a nonresonant tunnelling transport through the molecular junction, the current is exponentially dependent on the SAM thickness and on the energy barrier height, thus any normal distribution of these parameters leads to a log-normal distribution of the current.[36] This dispersion of the measured current can be due to inhomogeneities in the molecular organization in the SAM and variations of the loading forces (previous experiments on alkyl SAMs show a small increase in the current by a factor ~1.7 for a loading force in the range of 20−30 nN).[37] Three peaks (Figures 4b,c) are clearly distinguished. For the pristine SAM, two peaks (coming from two sets of measurements on the same SAM) are superimposed and have a log-mean (log μ) of ~10^{-9} A, and a log-

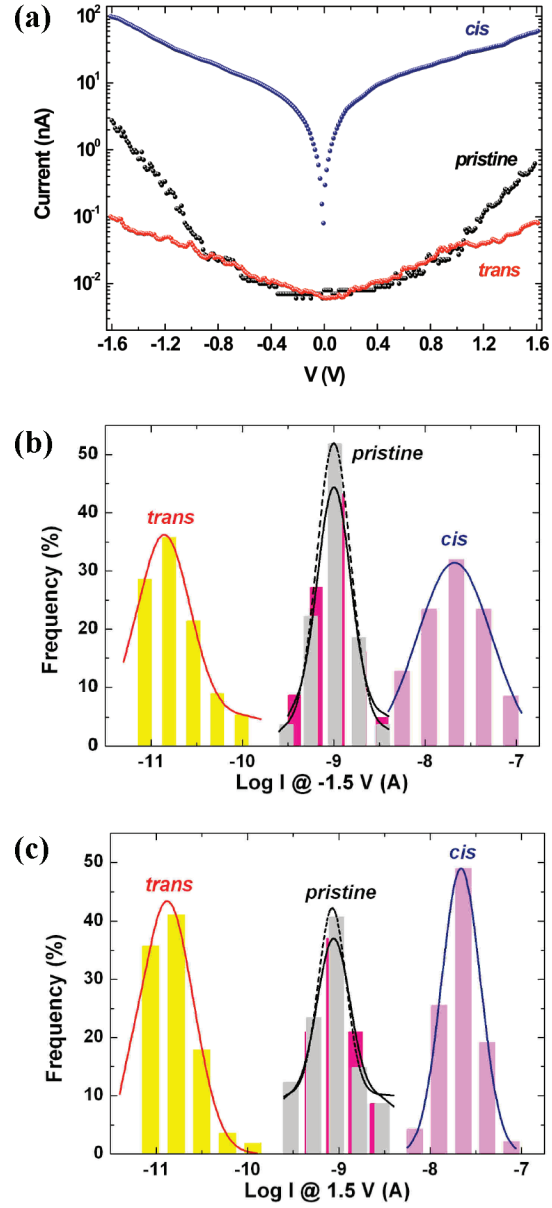

Figure 4. (a) Typical current (abs. value)−voltage (*I*−*V*) curves measured by C-AFM (load force 20−30 nN, voltage applied on the Au substrate of the sample) on a pristine SAM immediately after its formation, after irradiation at 360 nm during 90 min to switch the molecules in their cis isomer and after irradiation at 480 nm (90 min) to switch in the trans isomer. The curves are averaged over 10 *I*−*V* traces taken at the same C-AFM tip location. (b) Histograms of the current (in a log scale) for the same experiments (~40 *I*−*V* traces for each peaks). Three distinguishable log-normal distribution of the current are observed with log μ (log σ) values of ~10^{-9}(1.5), 1.4 × 10^{-11}(1.9), and 2.1 × 10^{-8}(2.45) A for the pristine SAM, trans and cis forms, respectively. (c) Same at 1.5 V with log μ (log σ) values of ~8.8 × 10^{-8}(1.5), 1.3 × 10^{-11}(1.9), and 2.2 × 10^{-8}(1.6) A for the pristine SAM, trans and cis forms, respectively.

standard deviation (log σ) of 1.5. After 90 min irradiation at 480 nm (formation of the trans isomer), the currents decrease and lead to a peak with log μ ≈ 1.4 × 10^{-11} A and log σ = 1.9. After 90 min irradiation at 360 nm (formation of the cis isomer), the current increases giving log μ = 2.1 × 10^{-8} A and log σ = 2.45 (all these

values at $V = -1.5$ V, similar values are obtained at $V = 1.5$ V, see Figure 4c). From these histograms, we deduce an on/off ratio with $\log \mu \approx 1.5 \times 10^3$ and $\log \sigma = 4.7$. It means that 68% of the devices has an on/off ratio between 320 and 7×10^3.[36] As for the case of contact angle and ellipsometry measurements, we observe intermediate values of the current for the pristine SAM, suggesting that just after its formation, the SAM contains a mixture of the two isomers. These measurements allow us to associate the cis isomer to the on state and trans isomer to the off state. We repeated these experiments at a macroscopic scale using eutectic GaIn drop contact (see Experimental Section). We qualitatively reproduced these results (see Supporting Information). We note that the C-AFM $I-V$ curves are almost symmetric while the molecule itself and the contacts (chemisorbed on one side and mechanical at the tip side) are asymmetric. It has been shown that asymmetries in the molecular junction produce asymmetric $I-V$.[38−40] However, the chemisorbed Au−S contact is separated from the azobenzene−thiophene moiety by a four-carbon atom saturated chain, and we surmize that this short alkyl chain can act as an additional contact resistance that counterbalances the contact asymmetry with respect to the more resistive mechanical molecule-tip side, leading to almost symmetrical $I-V$ curves.

Electronic Structures and First Principles Calculations. To explain the high switching ratio, we analyzed the $I-V$ traces in the cis and trans isomers with the transition voltage spectroscopy (TVS) method.[41] Recent works show that the TVS method gives a good determination of the position of the molecular orbitals with respect to the Fermi energy of the electrodes.[42,43] Figures 5a,b show typical $I-V$ curves (C-AFM contact) plotted as ln (I/V^2) *vs* $1/V$ for the negative and positive voltages. The bias (V_T) at the minimum of ln (I/V^2) directly determines the energy offset $\Phi = e|V_T|$ between the Fermi energy in the electrodes (the reference of energy being the Fermi energy at the grounded electrode) and the frontier orbitals of the molecules (whether it is the LUMO or HOMO is discussed below). Figure 5c shows the corresponding histograms for V_T (at both positive and negative biases) well fitted by a normal distribution. At negative bias, we get an energy offset $\Phi_{trans} \approx 1.76(\pm 0.08)$ eV and $\Phi_{cis} \approx 1.37(\pm 0.16)$ eV for the trans and cis isomers, respectively—these values are the mean values(standard deviation) of the fitted normal distribution shown in Figure 5c. At positive bias, we have $\Phi_{trans} \approx 1.91(\pm 0.04)$ eV and $\Phi_{cis} \approx 1.54(\pm 0.18)$ eV. The general trend is a reduction of the energy offset for the cis isomer. In previous works,[4,8] the increase in the conductance of the junction for the cis isomer was explained by a reduction in the tunnelling barrier length, that is, the length of the molecule. Assuming the same tunnel decay factor β of about 0.45 Å^{-1} for the two isomers in the classical expression of the conductance for a nonresonant tunnelling transport, $G = G_0 \exp(-\beta d)$, these authors consistently explained the switching ratio of about 25−30 observed in their experiments (G is the conductance, G_0 is an effective contact conductance and d is the tunnel barrier thickness, which is the thickness of the SAM). This approach is no longer valid in our case. Explaining a switching ratio $>1.5 \times 10^3$ would require a β value >1.3 Å^{-1}, a too high value for a conjugated molecule (β ≈ 0.4−0.6 Å^{-1} for conjugated molecules and 0.8−1 Å^{-1} for saturated molecules, *i.e.* alkyl chains).[44] Moreover, β depends on the tunnelling barrier height, and our observation of a change of Φ definitively excludes the hypothesis of a constant β value. The expression of the tunnelling de-

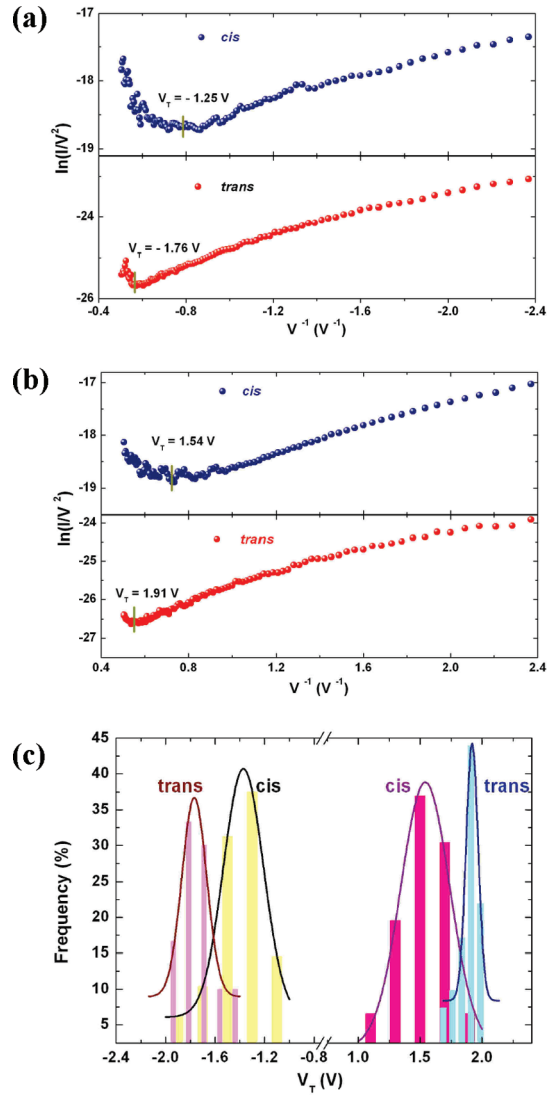

Figure 5. Plots of ln (I/V^2) versus $1/V$ for the cis and trans configurations at (a) negative and (b) positive voltages. (c) Histograms of the transition voltage V_T (voltage at the minimum of the ln (I/V^2) which determines the energy offset $\Phi = e|V_T|$. For C-AFM measurements, at negative voltages, the normal distribution (lines) gives $\Phi_{trans} = 1.76(\pm 0.08)$ eV—mean value μ with the standard deviation σ in brackets—for the trans isomer and $\Phi_{cis} = 1.37(\pm 0.16)$ eV for the cis isomer. At positive bias, we get: $\Phi_{trans} = 1.91(\pm 0.04)$ eV and $\Phi_{cis} = 1.54(\pm 0.18)$ eV.

cay factor β is usually related to barrier height Φ by $\beta = (2(2m_0\Phi)^{1/2}/\hbar)\alpha$ where m_0 is the electron mass, e the electron charge, $\hbar$ the reduced Planck constant, and α is an unitless factor accounting for the tunnelling energy barrier shape and/or an effective mass (since we do not know the detail of the potential shape and the effective mass in the junction, $m^* = \alpha^2 m_0$, we take $\alpha = 1$ which stands for a rectangular barrier and $m^* = m_0$).[45,46] Assuming the same α value and pre-exponential contact conductance G_0 for the two isomers, and taking into account both the changes in the energy barrier and the barrier thickness, the current ratio is given by

$$\frac{I_{cis}}{I_{trans}} = \exp\left(\frac{2\sqrt{2m_0\alpha}}{\hbar}(d_{trans}\sqrt{\Phi_{trans}} - d_{cis}\sqrt{\Phi_{cis}})\right) \quad (1)$$

With the data previously measured by ellipsometry ($d_{cis} \approx 25$ Å; $d_{trans} \approx 29$ Å) and TVS ($\Phi_{cis} \approx 1.54$ eV; $\Phi_{trans} \approx 1.91$ eV, see Figure 5), this ratio is estimated to about 2.1×10^3. This value is in good agreement with the experimental one; despite being a crude estimation. The calculated value is highly sensitive to the numerical values in the exponential function, for example if we take $d_{trans} = 30$ Å (the error bar is ±1 Å for the ellipsometry), the ratio increases to about 7.6×10^3. However, all these estimated numbers are in agreement with the range of the experimental data (68% of the devices has an on/off ratio between 3.2×10^2 and 7×10^3, see Figure 4). If $\alpha_{trans} \approx \alpha_{cis}$ seems reasonable, there is no reason to have the same G_0 for the two isomers. With the molecules in the trans isomer, the C-AFM tip is mostly in contact with the terminal CH_3 group, while it is mainly in contact with the N═N bonds or the phenyl rings for the cis isomer. Since it is known that a saturated bond acts as a tunnel barrier,[47−49] the molecules are more weakly coupled electronically with the contact in that case (see DFT calculation below), and it is likely that $G_{0,cis} > G_{0,trans}$. This feature will further increase the cis/trans ratio. We believe that this feature can explain the larger ratio than that in the previous experiments of Mativetsky and co-workers.[4] In the cis conformer, in both experiments the C-AFM tip is mainly in contact with the N═N bond. These authors have measured a current of $\sim 10^{-9}$ A (at ±0.3 V) while we have $\sim 7 \times 10^{-9}$ A at the same bias (Figure 4a). Since the same tip (PtIr with same radius of ~20 nm) has been used, our larger value can be due to the higher load force in our experiments. For instance, an increase by a factor *ca.* 5−10 has been measured between 2 (as in Mativetsky's work) and 20−30 nN (used here, see Experimental Section) in previous C-AFM experiments.[37] It is difficult to push the comparison further since the molecules used in the two experiments do not have exactly the same length, but we can conclude that the conductances G_{cis} are of the same order of magnitude in the two cases. In the trans isomer, we measured $\sim 10^{-11}$ A (at ±0.3 V), or equivalently *ca.* $(1-2) \times 10^{-12}$ A (renormalized at 2 nN) while Mativetsky *et al.* reported *ca.* $(7-8) \times 10^{-11}$ A, that is, a conductance G_{trans} higher by a factor 35−80. Thus, the high on/off ratio in our experiments may be explained by the strong decrease of G_{trans} due to the presence, between the phenyl and the tip, of a CH_3 end-group acting as a tunnel barrier, while the tip is directly in contact with the phenyl group in the work of Mativetsky and co-workers. In other words, the contact conductance is larger in the cis than in the trans isomer ($G_{0,cis} > G_{0,trans}$). It is difficult to estimate these values without the help of specific experiments, usually done by measuring the conductance *versus* the length of a molecule and extrapolating at a null length. In the case of more simple molecules (alkyl chains) a factor 10−100 has been measured between the contact conductance of a chemisorbed contact and a physisorbed one.[50] If we assume $G_{0,cis} \approx G_{0,trans}$ in the experiments of Mativetsky *et al.*,[4] we can crudely estimate $G_{0,cis}/G_{0,trans} \approx 35-80$ as discussed above, a factor that can account for a part of the overall $(1.5-7) \times 10^3$ cis/trans ratio reported here. Nevertheless, contacts are full parts of the molecular device and we conclude that the high cis/trans ratio measured here is an intrinsic phenomenon due to configurationaly induced changes in the electronic structure of the metal−molecule−metal junction. This can be consistently explained by a combination of the variation of the SAM thickness, change in the electronic structure of the metal−molecules−metal junction, and change in the molecule−electrode coupling.

To probe this later hypothesis further, we performed first principles DFT calculations (see Experimental Section). Three main DFT results support the higher conductance of the cis isomer: (i) The frontier orbitals are more delocalized in the cis isomer than in the trans (Figure 6). (ii) In the cis state, the molecule is more strongly coupled with the electrode as evidenced by the presence of a stronger wave function mixing and the higher charge transfer (+0.38 electron on Au) than in the trans state (+0.26 e). (iii) The energy offset between the Fermi energy and the LUMO is reduced by at least 0.53 eV when the molecule switches from the trans to cis isomer (Figure 6). Although a direct comparison of this last value to the experimental one remains delicate,[51] the trend is consistent with the experimental observation of a reduction of the energy tunnel barrier height. The discrepancy between experiment and theory is more probably related to the fact that a single molecule is used for the calculation and then molecule−molecule interactions are not taken into account. It is known that such interaction leads to a reduction of the HOMO−LUMO gap.[52] Inversely, the energy offset between the Au Fermi energy and HOMO slightly increases when switching from trans to cis (Figure 6).

Switching Kinetics. Finally, we investigated the switching kinetics by following the time-dependent evolutions of the current (for practical reasons, we measured

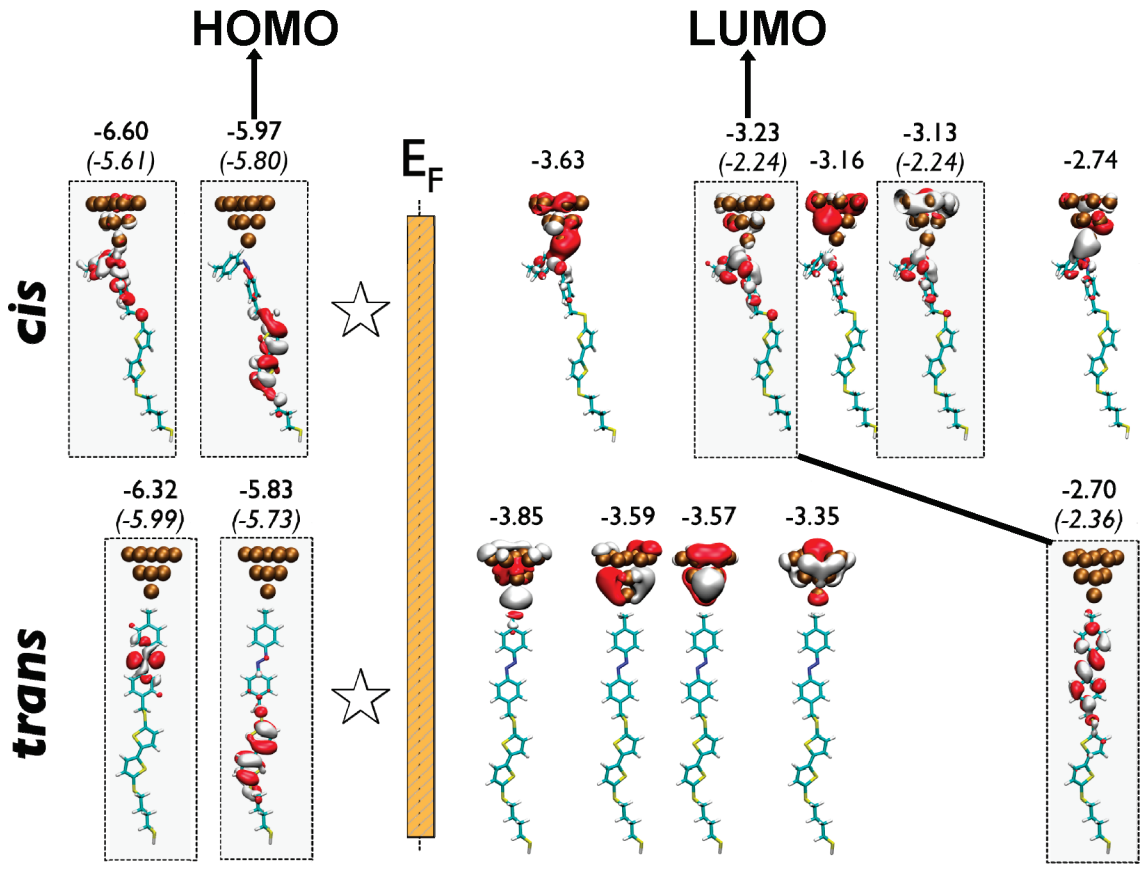

Figure 6. DFT calculations. Localization of the main frontier molecular orbitals (MOs) for the trans and cis isomers contacted by a gold tip as obtained by DFT calculations. We identified the MOs that originate from frontier MOs of isolated molecule by a light gray box. The star symbol indicates that two MOs centered on the Au11 electrode are not shown here. The DFT energy levels are given (in eV) for the couple Au/molecule while values in parentheses are the calculated levels for the isolated molecule.

the kinetics with the eGaIn drop, see Experimental Section) under irradiation by blue and UV lights. Before recording the kinetics of the trans-to-cis (cis-to-trans) isomerization under illumination with UV (or blue) light, the sample was submitted to lighting for 3 h with the blue (or UV) light so as to maximize the population of trans(cis) isomers, respectively. Each kinetic curve was measured with the same eGaIn tip. The following procedure was repeated: the tip was raised, the surface irradiated for 10 min, and the tip was lowered and put in contact with the surface to measure the $I-V$ characteristic. Since we did not use transparent substrate, the light irradiation and the $I-V$ measurements were not performed simultaneously. From these measurements, we generated the kinetic curves shown in Figure 7. Under UV light exposure (trans-to-cis), we can distinguish two exponential rate equations with characteristic time constants of 11 $\pm$ 1 min and 90 $\pm$ 8 min. Under blue light (cis-to-trans) only one is observed with a value of 20 $\pm$ 1 min. Note that this ratio of about 4.5 is consistent with the difference in light power density (70 μW/cm^2 for UV and 250 μW/cm^2 for blue lights, respectively). However, the shortest time constant under UV light concerns only a small fraction of the current (*i.e.*, a small number of molecules in the SAM) and, in the following, we concentrate on the slowest one which is the limiting factor. We determined the photonization cross-section by solving the usual first-order rate equations (master equations) given the fraction of molecules in the cis (C) and trans (T) conformation:

$$\begin{aligned} \frac{\partial C}{\partial t} &= \varphi T \sigma_{TC} - \varphi C \sigma_{CT} \\ \frac{\partial T}{\partial t} &= \varphi C \sigma_{CT} - \varphi T \sigma_{TC} \end{aligned} \qquad (2)$$

where φ is the photon flux and σ_{TC} and σ_{CT} are the trans-to-cis and cis-to-trans photoisomerization cross sections, respectively. This equation can be solved to give the following for UV light irradiation with initial boundary conditions $C = 0$ and $T = 1$,

$$C = \frac{\sigma_{TC}}{\sigma_{TC} + \sigma_{CT}}(1 - e^{-(\sigma_{TC}+\sigma_{CT})n}) \qquad (3)$$

and the following for blue light irradiation with initial boundary conditions $C = 1$ and $T = 0$,

$$T = \frac{\sigma_{CT}}{\sigma_{TC} + \sigma_{CT}}(1 - e^{-(\sigma_{TC}+\sigma_{CT})n}) \qquad (4)$$

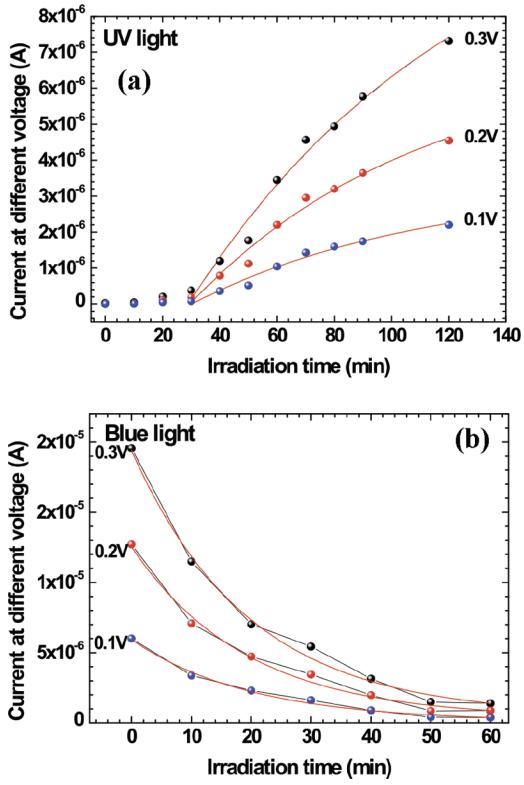

Figure 7. Evolution *versus* time of the current measured at different voltages (0.3, 0.2, and 0.1 V) under light exposition: (a) UV, trans-to-cis isomerization and (b) blue light, cis-to-trans isomerization. The lines correspond to the fits with a first-order rate equation (see text). Under, the UV light, the first 30 min are not taken into account (see text).

where the photon flux and time irradiation are combined to give the photon exposure $n = \varphi t$ (total number of photons per unit area). To determine C and T shown in Figure 8, we assume that the measured current is roughly proportional to the density of molecules in the cis conformation. Thus, we deduced $C(t)$ from data in Figure 7a by $C(t) = I(t)/I_\infty$ and $T(t)$ from data

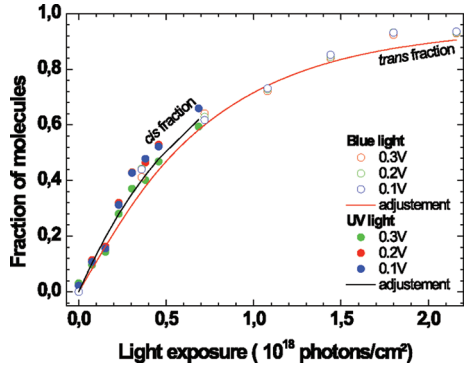

Figure 8. Evolution of the population of molecules in the cis and trans isomers as a function of the flux of photons irradiating the samples under a UV light (360 nm) and a blue light (480 nm), respectively. Before recording the trans to cis kinetics (at 360 nm), we illuminated the sample at 480 nm during 3 h to maximize the population of molecules in the trans isomer, and inversely before recording the cis to trans kinetics. The lines are the best fits of eqs 3 and 4 with the photoionization cross sections given in Table 1

TABLE 1. Values of the Trans-to-Cis σ_{TC} and Cis-to-Trans σ_{CT} Photoionization Cross Sections. In Our Experiments, Uncertainties Represent the Dispersion for Measurements Taken at Various Voltages Applied on the Samples

	σ_{TC} (cm²)	σ_{CT} (cm²)	refs
UV light (360 nm)	$(1.5 \pm 0.2) \times 10^{-18}$	$(5.4 \pm 2.0) \times 10^{-20}$	this work
	2.3×10^{-23}	2.3×10^{-23}	53
	$(4 \pm 1) \times 10^{-18}$		54
blue light (480 nm)	$(3.9 \pm 0.8) \times 10^{-20}$	$(1.4 \pm 0.2) \times 10^{-18}$	this work
	1.7×10^{-23}	2.3×10^{-23}	53
		$(2.5 \pm 0.9) \times 10^{-19}$	54

in Figure 7b by $T(t) = 1 - I(t)/I_0$ where I_0 is the current at $t = 0$ and I_∞ is the saturation current extrapolated from data in Figure 7a. $C(t)$ and $T(t)$ *versus* n are given in Figure 8 and fitted with eqs 3 and 4. Considering that $C = 0$, $T = 1$, and all molecules trans as the initial conditions of the kinetics equations under UV-light (trans-to-cis) and $C = 1$, $T = 0$, and all molecules cis under blue-light (cis-to-trans) is a strong hypothesis. While we cannot exclude that a fraction of molecules in the SAMs cannot switch, or that the cis-to-trans and trans-to-cis transformation are incomplete, these initial conditions seem reasonable according to thickness measurements by ellipsometry (see above, Monolayer Formation and Characterization). Table 1 gives the fitted (fits are the full lines in Figure 8) values of σ_{TC} and σ_{CT}. They are compared with the values of two others experiments on monolayers of azobenzene derivatives.[12,53,54] Our values are very close to those measured by sum-frequency generation vibrational spectroscopy on a SAM of azobenzene linked to Au surface through a linker system composed of a tripodal unit and an adamantane core.[54] Compared to the data in ref 53, we obtain larger photoionization cross sections and a clear asymmetrical behavior, $\sigma_{TC} > \sigma_{CT}$ under UV light and $\sigma_{CT} > \sigma_{TC}$ under blue light, whereas $\sigma_{CT} \approx \sigma_{TC}$ in ref 53. This feature may be due to differences in the molecular arrangement in the monolayers in both experiments. In ref 53, the azobenzenes are lying flat on the surface and are decoupled by short (≈ 3.2 Å) *tert*-butyl legs. On the contrary, in our case, as in ref 54, the photoisomerizable azobenzene is strongly "mechanically" and "electronically" decoupled from the metal surface by a long linker (≈ 14 Å for the four-carbon atom alkyl and the bithiophene), and the measured photoionization cross sections are on a par with the known value for the azobenzene family in solution. Such results illustrate the important role of the spacer in the dynamical behavior of azobenzene derivatives self-assembled on a solid surface.

CONCLUSIONS

Self-assembled monolayers of a new azobenzene−thiophene derivative exhibit high on/off conductance ratio upon configurational change, with

the higher conductance state associated to a cis isomer of the azobenzene moiety. In the framework of a nonresonant tunneling transport through the metal−molecule−metal (at low bias) this ratio is satisfactorily explained by considering a combined modification of both the tunnel barrier length (*i.e.*, decrease in the length of the molecule in the cis form) and a lowering of the energy position of the LUMO with respect to the electrode Fermi energy for the cis isomer. First principles DFT calculations support our conclusions and clearly demonstrate a better delocalization of frontier orbitals, as well as a stronger electronic coupling between the azobenzene moiety and the electrodes, in the cis configuration rather than in the trans one. These results allow us to envision these molecules as building blocks for fast (with $\sigma \approx 10^{-18}$ cm^2 switching time *ca.* 1−10 μs could be achieved, in principle, with a high intensity light source) solid-state molecular switch and memory devices with a high on/off conductance ratio.

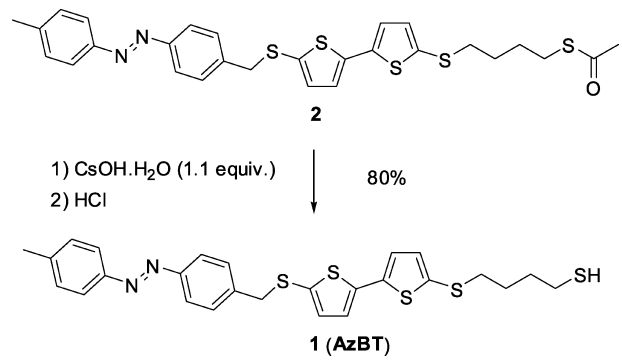

Scheme 1. Chemical structures of the molecules.

EXPERIMENTAL SECTION

Synthesis of the Self-Assembled Monolayers. The synthesis of titled compound **1** (AzBT) is obtained in 80% yields from precursor **2** after a saponification reaction of the thioester group by treatment with cesium hydroxide followed by the addition of hydrochloric acid (Scheme 1). Details on the synthesis and characterization of these molecules are given elsewhere.[55]

We prepared gold Au(111) substrates by evaporating 10 nm of titanium to promote adhesion and 100 nm of gold onto cleaned silicon substrate using an e-beam evaporator. We used a low deposition rate (1 Å · s^{-1}) at 10^{-8} Torr to minimize the roughness. Before grafting the molecules, we cleaned the Au substrates by piranha attack ($^1/_3$ H_2O_2 30% and $^2/_3$ concentrated H_2SO_4 96%) during 15 min, followed by an immersion in a dilute aqua regia solution (3:1:16 HCl 37%:HNO_3 65%:H_2O) during 5 min to reduce gold roughness (≈ 1.7 nm rms). For the SAM fabrication, we exposed this freshly cleaned gold surface to 1 mM solution of **1** in dichloromethane during 72 h. The reaction took place in a glovebox with a controlled atmosphere (N_2 with <1 ppm of water and oxygen) and in the dark. Then, we rinsed the treated substrates with dichloromethane followed by a cleaning in an ultrasonic bath of dichloromethane during 5 min. A stable cyclic voltammetry (CyV) trace of monolayer of **1** exhibits a reversible one-electron oxidation wave at $E_{pa}{}^1 = 0.98$ V associated with a reduction peak potential at 0.95 V measured during the reduction back sweep. CyV analysis of the monolayer has been carried out at different scan rates ranging from 50 to 8000 mV/s. The linear variation of the peak current *versus* scan rate and the invariance of $E_{pa}{}^1 = 0.98$ V with scan rate confirm that molecules **1** are immobilized on the electrode surface. The surface coverage has been determined by integration of the voltammetric peak after correction for double layer charge. A value of *ca.* 4 × 10^{-10} mol · .cm^{-2} was obtained for the monolayer of **1**, indicative of a densely close-packed monolayer.

Contact-Angle Measurements. We measured the water contact angle with a remote-computer controlled goniometer system (DIGIDROP by GBX, France). We deposited a drop (10−30 μL) of deionized water (18MΩ · cm^{-1}) on the surface, and the projected image was acquired and stored by the computer. Contact angles were extracted by contrast contour image analysis software. These angles were determined a few seconds after application of the drop. These measurements were carried out in a clean room (ISO 6) where the relative humidity (50%) and the temperature (22 °C) are controlled. The precision with these measurements are ±2°.

Spectroscopic Ellipsometry. We recorded spectroscopic ellipsometry data in the visible range using an UVISEL (Jobin Yvon Horiba) spectroscopic ellipsometer equipped with a DeltaPsi 2 data analysis software. The system acquired a spectrum ranging from 2 to 4.5 eV (corresponding to 300−750 nm) with intervals of 0.1 eV (or 15 nm). Data were taken at an angle of incidence of 70°, and the compensator was set at 45.0°. We fitted the data by a regression analysis to a film-on-substrate model as described by their thickness and their complex refractive indexes. First, we recorded a background before monolayer deposition for the gold-coated substrate. Second, after the monolayer deposition, we used a two-layer model (substrate/SAM) to fit the measured data and to determine the SAM thickness. We used the previously measured optical properties of the gold-coated substrate (background), and we fixed the refractive index of the organic monolayer at 1.50. The usual values in the literature for the refractive index of organic monolayers are in the range 1.45−1.50.[56,57] We can notice that a change from 1.50 to 1.55 would result in less than 1 Å error for a thickness less than 30 Å. We estimated the accuracy of the SAM thickness measurements at ±1 Å.

XPS Measurements. We performed XPS measurements to control the chemical composition of the SAMs and to detect any contaminant. We used a Physical Electronics 5600 spectrometer fitted in an UHV chamber with a residual pressure of 2 × 10^{-10} Torr. High resolution spectra were recorded with a monochromatic Al Kα X-ray source (hυ = 1486.6 eV), a detection angle of 45° as referenced to the sample surface, an analyzer entrance slit width of 400 mm and with an analyzer pass energy of 12 eV. In these conditions, the overall resolution as measured from the full-width half-maximum (fwhm) of the Ag $3d_{5/2}$ line is 0.55 eV. Semiquantitative analyses were completed after standard background subtraction according to Shirley's method.[58] Peaks were decomposed by using the Voigt functions and a least-squares minimization procedure and by keeping constant the Gaussian and Lorentzian broadenings for each component of a given peak.

Electrical Measurements. We performed current−voltage measurements by conducting atomic force microscopy (C-AFM) in ambient air (Dimension 3100, Veeco), using a PtIr coated tip (tip radius of curvature less than 25 nm, force constant in the range 0.17−0.2 N/m). Placing the conducting tips at a stationary point contact formed nanojunctions. A square grid of 10 × 10 is defined with a lateral step of 2 nm. At each point, 10 *I*−*V* curves are acquired and averaged. Out of the 100 *I*−*V* traces, some are eliminated due to lateral drift of the C-AFM setup and about 40 *I*−*V* "mechanically stable" traces are used for statistics. The load force was adjusted in the range 20−30 nN and measured by force−distance curves with the controlling software of the Dimension 3100. The bias was applied on the Au substrate, and the tip was grounded through the input of the current amplifier. We focused the light from a xenon lamp to an optical fiber. We used two dichroic filters centered at 360 and 480 nm. At the output of the optical filter, the SAMs were irradiated on about 1 cm^2 at power density of 70 μW/c^2 (at 360 nm) and 250 μW/c^2 (at 480 nm). Because of the size and design of the Dimension 3100, it is not easily possible to bring the optical fiber close to the C-AFM tip, thus the light irradiation was not done with the C-AFM tip contacting the monolayer. We moved the sample

mounted on the chuck back and forth between AFM tip area and the illumination area located nearby on the Dimension 3100 platform. We also used Eutectic GaIn drop contact (eGaIn 99.99%, Ga:In; 75.5:24.5 wt % from Alfa Aesar). We used a method close to the one developed by Chiechi *et al.*[59] We formed a drop of eGaIn at the extremity of a needle fixed on a micromanipulator. By displacing the needle, we brought the drop into contact with a sacrificial surface, and we retracted the needle slowly. By this technique, we formed a conical tip of eGaIn with a diameter ranging from 50 to 200 μm (corresponding to contact area ranging from 10^{-5} to 10^{-3} cm^2). This conical tip was then put into contact with SAM (under control with a digital video camera). Voltage was applied on the eGaIn drop. The contact area was also determined by measuring the 1 MHz capacity of the junction and assuming a relative permittivity of $\varepsilon_R = 2.2$ for the SAM.

First Principles Calculations. Quantum chemical density functional theory (DFT) calculations were performed with the NWChem software package.[60] We used a 6-31G basis set for carbon, nitrogen, sulfur, and hydrogen atoms in conjunction with the B3LYP functional for exchange and correlation. For gold atoms, the LANL2DZ basis set was used to describe the 19 valence and 60 core electrons. The isolated molecular structure of the AzBT was fully optimized without symmetry constraints using the quasi-Newton method until a gradient convergence factor better than 10^{-5} Hartree/Bohr was reached. Several starting geometries were considered during this optimization process, and only the most stable final structures (cis and trans) were conserved. The electronic structures of the Au_{11}-AzBT ($^2A_1$ states) were obtained from the optimized AzBT molecule where we placed a fixed Au_{11} cluster at virtually the same distance (0.2 nm) from cis or trans AzBT molecule. The relative stability of the species was calculated with respect to the ground state geometry.

Acknowledgment. This work was financially supported by ANR-PNANO under the OPTOSAM project (No. ANR-06-NANO-016).

Supporting Information Available: Current−voltage curves at a macroscopic scale (Hg drop) and corresponding discussion; Figures S1 and S2. This material is available free of charge *via* the Internet at http://pubs.acs.org.

REFERENCES AND NOTES

1. Katsonis, N.; Lubomska, M.; Pollard, M. M.; Feringa, B.; Rudolf, P. Synthetic Light-Activated Molecular Switches and Motors on Surfaces. *Prog. Surf. Sci.* **2007**, *82*, 407–434.
2. Kronemeijer, A. J.; Akkerman, H. B.; Kudernac, T.; van Wees, B. J.; Feringa, B.; Blom, P. W. M.; de Boer, B. Reversible Conductance Switching in Molecular Devices. *Adv. Mater.* **2008**, *20*, 1467–1473.
3. Kumar, A. S.; Ye, T.; Takami, T.; Yu, B.-C.; Flatt, A. K.; Tour, J. M.; Weiss, P. S. Reversible Photoswitching of Single Azobenzene Molecules in Controlled Nanoscale Environments. *Nano Lett.* **2008**, *8*, 1644–1648.
4. Mativetsky, J. M.; Pace, G.; Elbing, M.; Rampi, M. A.; Mayor, M.; Samori, P. Azobenzenes as Light-Controlled Molecular Electronic Switches in Nanoscale Metal−Molecule−Metal Junctions. *J. Am. Chem. Soc.* **2008**, *130*, 9192–9193.
5. Wen, Y.; Yi, W.; Meng, L.; Feng, M.; Jiang, G.; Yuan, W.; Zhang, Y.; Gao, H.; Jiang, L.; Song, Y. Photochemical-Controlled Switching Based on Azobenzene Monolayer Modified Silicon (111) Surface. *J. Phys. Chem. B* **2005**, *109*, 14465–14468.
6. van der Molen, J. S.; Liao, J.; Kudernac, T.; Agustsson, J. S.; Bernard, L.; Calame, M.; van Wees, B. J.; Feringa, B. L.; Schönenberger, C. Light-Controlled Conductance Switching of Ordered Metal−Molecule−Metal Devices. *Nano Lett.* **2009**, *9*, 76–80.
7. Zhang, X.; Wen, Y.; Li, Y.; Li, G.; Du, S.; Guo, H.; Yang, L.; Jiang, L.; Gao, H.; Song, Y. Molecularly Controlled Modulation of Conductance on Azobenzene Monolayer-Modified Silicon Surfaces. *J. Phys. Chem. C* **2008**, *112*, 8288–8293.
8. Ferri, V.; Elbing, M.; Pace, G.; Dickey, M. D.; Zharnikov, M.; Samori, P.; Mayor, M.; Rampi, M. A. Light-Powered Electrical Switch Based on Cargo-Lifting Azobenzene Monolayers. *Angew. Chem., Int. Ed.* **2008**, *47*, 3407–3409.
9. Delorme, N.; Bardeau, J. F.; Bulou, A.; Poncin-Epaillard, F. Azobenzene-Containing Monolayer with Photoswitchable Wettability. *Langmuir* **2005**, *21*, 12278–12282.
10. Wan, P.; Jiang, Y.; Wang, Y.; Wang, Z.; Zhang, X. Tuning Surface Wettability Through Photocontrolled Reversible Molecular Shuttle. *Chem. Commun.* **2008**, *44*, 5710–5712.
11. Dietrich, P.; Michalik, F.; Schmidt, R.; Gahl, C.; Mao, G.; Breusing, M.; Raschke, M.; Priewisch, B.; Elsässer, T.; Mendelsohn, R.; *et al.* An Anchoring Strategy for Photoswitchable Biosensor Technology: Azobenzene-Modified SAMs on Si(111). *Appl. Phys. A* **2008**, *93*, 285–292.
12. Comstock, M. J.; Levy, N.; Kirakosin, A.; Cho, J.; Lauterwasser, F.; Harvey, J. H.; Strubbe, D. A.; Fréchet, J. M. J.; Trauner, D.; Louie, S. G.; *et al.* Reversible Photomechanical Switching of Individual Engineered Molecules at a Metallic Surface. *Phys. Rev. Lett.* **2007**, *99*, 038301.
13. Suda, M.; Kameyama, N.; Ikegami, A.; Einaga, Y. Reversible Phototuning of the Large Anisotropic Magnetization at the Interface between a Self-Assembled Photochromic Monolayer and Gold. *J. Am. Chem. Soc.* **2008**, *131*, 865–870.
14. Ahonen, P.; Laaksonen, T.; Schiffrin, D. J.; Kontturi, K. Photoswitching Electron Transport Properties of an Azobenzene Containing Thiol-SAM. *Phys. Chem. Chem. Phys.* **2007**, *9*, 4898–4901.
15. Katsonis, N.; Kudernac, T.; Walko, M.; Van der Molen, S.; Van Wees, B.; Feringa, B. Reversible Conductance Switching of Single Diarylethenes on a Gold Surface. *Adv. Mater.* **2006**, *18*, 1397–1400.
16. Dulic, D.; van der Molen, S. J.; Kudernac, T.; Jonkman, H. T.; de Jong, J. J. D.; Bowden, T. N.; van Esch, J.; Feringa, B. L.; van Wees, B. J. One-Way Optoelectronic Switching of Photochromic Molecules on Gold. *Phys. Rev. Lett.* **2003**, *91*, 207402.
17. del Valle, M.; Gutierrez, R.; Tejedor, C.; Cuniberti, G. Tuning the Conductance of a Molecular Switch. *Nat. Nanotechnol.* **2007**, *2*, 176–179.
18. Zhang, C.; Du, M. H.; Cheng, H. P.; Zhang, X. G.; Roitberg, A. E.; Krause, J. L. Coherent Electron Transport Through an Azobenzene Molecule: A Light-Driven Molecular Switch. *Phys. Rev. Lett.* **2004**, *92*, 158301.
19. Zhang, C.; He, Y.; Cheng, H.-P.; Xue, Y.; Ratner, M. A.; Zhang, X. G.; Krstic, P. Current−Voltage Characteristics Through a Single Light-Sensitive Molecule. *Phys. Rev. B* **2006**, *73*, 125445.
20. Yasuda, S.; Nakamura, T.; Matsumoto, M.; Shigekawa, H. Phase Switching of a Single Isomeric Molecule and Associated Characteristic Rectification. *J. Am. Chem. Soc.* **2003**, *125*, 16430–16433.
21. Nozaki, D.; Cuniberti, G. Silicon-Based Molecular Switch Junctions. *Nano Res.* **2009**, *2*, 648–659.
22. Vance, L.; Willey, T. M.; Nelson, A. J.; van Buuren, T.; Bostedt, C.; Terminello, L. J.; Fox, J. A. XAS and XPS Characterization of Monolayers Derived from a Dithiol and Structurally Related Disulfide-Containing Polyamides. *Langmuir* **2002**, *18*, 8123–8128.
23. Bourg, M. C.; Badia, A.; Lennox, R. B. Gold−Sulfur Bonding in 2D and 3D Self-Assembled Monolayers: XPS Characterization. *J. Phys. Chem. B* **2000**, *104*, 6562–6567.
24. Beulen, M. W. J.; Bugler, J.; Lammerink, B.; Geurts, F. A. J.; Biemond, M. E. F.; van Leerdam, K. G. C.; van Veggel, F. C. J. M.; Engbersen, J. F. J.; Reinhoudt, D. N. Self-Assembled Monolayers of Heptapodant β-Cyclodextrins on Gold. *Langmuir* **1998**, *14*, 6424–6429.
25. Rieley, H.; Kendall, G. K.; Zemicael, F. W.; Smith, T. L.; Yang, S. X-ray Studies of Self-Assembled Monolayers on Coinage Metals. 1. Alignment and Photooxidation in 1,8-Octanedithiol and 1-Octanethiol on Au. *Langmuir* **1998**, *14*, 5147–5153.
26. Laibinis, P. E.; Whitesides, G. M.; Allara, D. L.; Tao, Y.-T.; Parikh, A. N.; Nuzzo, R. G. Comparison of the Structures and Wetting Properties of Self-Assembled Monolayers of *n*-Alkanethiols on the Coinage Metal Surfaces, Copper, Silver, and Gold. *J. Am. Chem. Soc.* **1991**, *113*, 7152–7167.

27. Castner, D. G.; Hinds, K.; Grainger, D. W. X-ray Photoelectron Spectroscopy Sulfur 2p Study of Organic Thiol and Disulfide Binding Interactions with Gold Surfaces. *Langmuir* **1996**, *12*, 5083–5086.
28. *CS MOPAC*; Cambridge Soft Corporation: Cambridge, MA, 1996.
29. Feng, C. L.; Qu, G.; Song, Y.; Jiang, L.; Zhu, D. Surface Arrangement of Azobenzene Moieties in Two Different Azobenzene-Derived Langmuir−Blodgett Films. *Surf. Interface Anal.* **2006**, *38*, 1343–1347.
30. El Garah, M.; Palmino, F.; Cherioux, F. Reversible Photoswitching of Azobenzene-Based Monolayers Physisorbed on a Mica Surface. *Langmuir* **2010**, *26*, 943–949.
31. Folkers, J. P.; Laibinis, P. E.; Whitesides, G. M. Self-Assembled Monolayers of Alkanethiols on Gold: Comparisons of Monolayers Containing Mixtures of Short- and Long-Chain Constituents with CH_3 and CH_2OH Terminal Groups. *Langmuir* **1992**, *8*, 1330–1341.
32. Ruslim, C.; Ichimura, K. Spectroscopic and Thermal Isomerization Characteristics of 3,3′-Dialkoxy and Dialkanoyloxy Azobenzenes. *J. Mater. Chem.* **2000**, *10*, 2704–2707.
33. Pace, G.; Ferri, V.; Grave, C.; Elbing, M.; von Hänisch, C.; Zharnikov, M.; Mayor, M.; Rampi, M. A.; Samori, P. Cooperative Light-Induced Molecular Movements of Highly Ordered Azobenzene Self-Assembled Monolayers. *Proc. Natl. Acad. Sci. U.S.A.* **2007**, *104*, 9937–9942.
34. Evans, S. D.; Johnson, S. R.; Ringsdorf, H.; Williams, L. M.; Wolf, H. Photoswitching of Azobenzene Derivatives Formed on Planar and Colloidal Gold Surfaces. *Langmuir* **1998**, *14*, 6436–6440.
35. Kim, T.-W.; Wang, G.; Lee, H.; Lee, T. Statistical Analysis of Electronic Properties of Alkanethiols in Metal−Molecule−Metal Junctions. *Nanotechnology* **2007**, *18*, 315204.
36. If X is a random variable with a normal distribution, then $Y = \exp(X)$ has a log-normal distribution; likewise, if Y is log-normally distributed, then $\log(Y)$ is normally distributed. If m and s are the mean value and standard deviation of normal distribution of $\log(Y)$, we denote $\log \mu$ the log-mean ($=10^m$) and $\log \sigma$ the log standard deviation ($=10^s$) of the log-normal distribution of Y. All results are given as $\log \mu(\log \sigma)$ unless otherwise specified. Thus, 68% of the measured data are between $\log \mu/\log \sigma$ and $\log \mu \times \log \sigma$.
37. Wold, D. J.; Frisbie, C. D. Fabrication and Characterization of Metal−Molecule−Metal Junctions by Conducting Probe Atomic Force Microscopy. *J. Am. Chem. Soc.* **2001**, *123*, 5549–5556.
38. Kushmerick, J. G.; Holt, D. B.; Yang, J. C.; Naciri, J.; Moore, M. H.; Shashidhar, R. Metal−Molecule Contacts and Charge Transport Across Monomolecular Layers: Measurement and Theory. *Phys. Rev. Lett.* **2002**, *89*, 086802.
39. Reichert, J.; Ochs, R.; Beckmann, D.; Weber, H. B.; Mayor, M.; Löhneysen, H. v. Driving Current through Single Organic Molecules. *Phys. Rev. Lett.* **2002**, *88*, 176804.
40. Lenfant, S.; Krzeminski, C.; Delerue, C.; Allan, G.; Vuillaume, D. Molecular Rectifying Diodes from Self-Assembly on Silicon. *Nano Lett.* **2003**, *3*, 741–746.
41. Beebe, J. M.; Kim, B.; Gadzuk, J. W.; Frisbie, C. D.; Kushmerick, J. G. Transition from Direct Tunneling to Field Emission in Metal−Molecule−Metal Junctions. *Phys. Rev. Lett.* **2006**, *97*, 026801.
42. Beebe, J. M.; Kim, B.; Frisbie, C. D.; Kushmerick, J. G. Measuring Relative Barrier Heights in Molecular Electronic Junctions with Transition Voltage Spectroscopy. *ACS Nano* **2008**, *2*, 827–832.
43. Huisman, E. H.; Guédon, C. M.; van Wees, B. J.; van der Molen, S. J. Interpretation of Transition Voltage Spectroscopy. *Nano Lett.* **2009**, *9*, 3909–3913.
44. Salomon, A.; Cahen, D.; Lindsay, S. M.; Tomfohr, J.; Engelkes, V. B.; Frisbie, C. D. Comparison of Electronic Transport Measurements on Organic Molecules. *Adv. Mater.* **2003**, *15*, 1881–1890.
45. Wang, W.; Lee, T.; Reed, M. A. Mechanism of Electron Conduction in Self-Assembled Alkanethiol Monolayer Devices. *Phys. Rev. B* **2003**, *68*, 035416.
46. Holmlin, R. E.; Haag, R.; Chabinyc, M. L.; Ismagilov, R. F.; Cohen, A. E.; Terfort, A.; Rampi, M. A.; Whitesides, G. M. Electron Transport through Thin Organic Films in Metal−insulator−metal Junctions Based on Self-Assembled Monolayers. *J. Am. Chem. Soc.* **2001**, *123*, 5075–5085.
47. Mann, B.; Kuhn, H. Tunneling through Fatty Acid Salt Monolayers. *J. Appl. Phys.* **1971**, *42*, 4398–4405.
48. Boulas, C.; Davidovits, J. V.; Rondelez, F.; Vuillaume, D. Suppression of Charge Carrier Tunneling through Organic Self-Assembled Monolayers. *Phys. Rev. Lett.* **1996**, *76*, 4797–4800.
49. Vuillaume, D.; Boulas, C.; Collet, J.; Allan, G.; Delerue, C. Electronic Structure of Alkylsiloxane Self-Assembled Monolayer−Silicon Heterostructure. *Phys. Rev. B* **1998**, *58*, 16491–16498.
50. Engelkes, V. B.; Beebe, J. M.; Frisbie, C. D. Length-Dependent Transport in Molecular Junctions Based on SAMs of Alkanethiols and Alkanedithiols: Effects of Metal Work Function and Applied Bias on Tunneling Efficiency and Contact Resistance. *J. Am. Chem. Soc.* **2004**, *126*, 14287–14296.
51. Although the behaviour of the small Au_{11} cluster should reproduce the main electronic features of an extended system, the determination of a comparable Fermi level to experiment would necessite the investigation of much larger clusters with converged electronic properties. In addition, we modeled the upper electrode (AFM tip or eGaIn) by a gold electrode which obviously cannot be directly compared to experimental data.
52. Cornil, J.; Beljonne, D.; Calbert, J. P.; Brédas, J. L. Interchain Interactions in Organic π-Conjugated Materials: Impact on Electronic Structure, Optical Response, And Charge Transport. *Adv. Mater.* **2001**, *13*, 1053–1067.
53. Comstock, M. J.; Levy, N.; Cho, J.; Berbil-Bautista, L.; Crommie, M. F.; Poulsen, D. A.; Frechet, J. M. J. Measuring Reversible Photomechanical Switching Rates for a Molecule at a Surface. *Appl. Phys. Lett.* **2008**, *92*, 123107–3.
54. Wagner, S.; Leyssner, F.; Kördel, C.; Zarwell, S.; Schmidt, R.; Weinelt, M.; Rück-Braun, K.; Wolf, M.; Tegera, P. Reversible Photoisomerization of an Azobenzene-Functionalized Self-Assembled Monolayer Probed by Sum-Frequency Generation Vibrational Spectroscopy. *Phys. Chem. Chem. Phys.* **2009**, *11*, 6242–6248.
55. Karpe, S.; Ocafrain, M.; Smaali, K.; Lenfant, S.; Vuillaume, D.; Blanchard, P.; Roncali, J., Oligothiophene-Derivatized Azobenzene as Immobilized Photoswitchable Conjugated Systems. Chem. Commun. **2010**, DOI: 10.1039/c002072a.
56. Parikh, A. N.; Allara, D. L.; Ben Azouz, I.; Rondelez, F. An Intrinsic Relationship between Molecular Structure in Self-Assembled *n*-Alkylsiloxane Monolayers and Deposition Temperature. *J. Phys. Chem.* **1994**, *98*, 7577–7590.
57. Ulman, A. *An Introduction to Ultrathin Organic Films: From Langmuir−Blodgett to Self-Assembly*; Academic: Boston, MA, 1991.
58. Shirley, D. A. High-Resolution X-ray Photoemission Spectrum of the Valence Bands of Gold. *Phys. Rev. B* **1972**, *5*, 4709–4714.
59. Chiechi, R. C.; Weiss, E. A.; Dickey, M. D.; Whitesides, G. M. Eutectic Gallium−Indium (EGaIn): A Moldable Liquid Metal for Electrical Characterization of Self-Assembled Monolayers. *Angew. Chem., Inter. Ed.* **2008**, *47*, 142–144.
60. Bylaska, E. J.; de Jong, W. A.; Govind, N.; Kowalski, K.; Straatsma, T. P.; Valiev, M.; Wang, D.; Apra, E.; Windus, T. L.; Hammond, J.; *et al. NWChem, A Computational Chemistry Package for Parallel Computers*, version 5.1.1; Pacific Northwest National Laboratory: Richland, WA, 2009.